Effective operators in two-nucleon systems

James P. Vary, Robert Basili, Weijie Du, Matthew Lockner, Pieter Maris, Soham Pal, and Shiplu Sarker
Department of Physics and Astronomy, Iowa State University, Ames, Iowa 50011, USA

(Received 9 September 2018; published 10 December 2018)

Effective Hamiltonians and effective electroweak operators are calculated with the Okubo-Lee-Suzuki formalism for two-nucleon systems. Working within a harmonic oscillator basis, first without and then with a confining harmonic oscillator trap, we demonstrate the effects of renormalization on observables calculated for truncated basis spaces. We illustrate the renormalization effects for the root-mean-square point-proton radius, electric quadrupole moment, magnetic dipole moment, Gamow-Teller transition, and neutrinoless double-β decay operator using nucleon-nucleon interactions from chiral effective field theory. Renormalization effects tend to be larger in the weaker traps and smaller basis spaces, suggesting applications to heavier nuclei with transitions dominated by weakly bound nucleons would be subject to more significant renormalization effects within achievable basis spaces.

DOI: 10.1103/PhysRevC.98.065502

I. INTRODUCTION

Precision studies of electroweak properties of nuclei have become of great interest to complement major advances underway in experimental nuclear physics. As an example, significant experimental and theoretical efforts are aimed at searches for neutrinoless double-β ($0\nu2\beta$) decay which require significant investments in new experimental facilities and in theoretical advances. Our limited goal here is to use solvable two-nucleon systems within a configuration-interaction (CI) approach in order to explore the dependence of electroweak operators on the CI basis-space truncation when evaluating nuclear properties. Information on the size of these effects can help interpret previous studies and guide plans for calculations in larger nuclei.

We select systems of two nucleons interacting via realistic nucleon-nucleon (NN) interactions both in free space and in a harmonic oscillator (HO) trap for investigating renormalization effects on a suite of electroweak properties. These systems are numerically solvable in a large HO basis space providing high precision results for comparison with approximate results. This allows us to map out the effects arising from the correlations governed by different interactions, as well as the effects due to basis-space truncation and the effects linked with the length scale of the environment, the trap. To accurately calculate these effects we adopt the Okubo-Lee-Suzuki (OLS) method [1–3] to derive the basis truncation dependence of effective interactions and operators. By comparing matrix elements of these derived effective operators with those from a truncated treatment of the original operators, we observe the truncation effects (conversely the renormalization effects) on each electroweak operator for each basis space and for each confining HO trap. While most effects tend to be in the range of a few percentages, the effects on the $0\nu2\beta$ matrix element can be above a factor of two for some systems. Such cases suggest a careful treatment of renormalization effects must be implemented for $0\nu2\beta$ decay matrix elements in limited basis spaces. Fortunately, these same OLS methods are adaptable to more realistic applications as in the case of the no-core shell model (NCSM) [4–7] and to valence space effective interactions as well [8].

This work may be viewed in the context of a related pioneering work that extensively investigated the deuteron and its electromagnetic form factors with renormalization group methods [9]. The importance of maintaining consistency in the renormalization of both the Hamiltonian and all other observables is the theme we share. The renormalization method, interactions, observables and presence of a trap distinguish our work from Ref. [9].

II. THEORETICAL FRAMEWORK

A. Many-body systems

We seek to solve a Hamiltonian H eigenvalue problem expressed in a suitable basis and, once the eigenvectors are obtained, to evaluate matrix elements of additional observables O. For nuclear physics applications, such as the NCSM, the resulting matrix for H is infinite dimensional. With truncation, the matrix of H becomes numerically tractable, allowing the study of results as a function of the finite basis parameters in order to estimate the converged results and their uncertainties. For the NCSM, we express H in terms of the relative kinetic energy operator $T_{\rm rel}$ acting between all pairs of nucleons in the A-nucleon system and an interaction term V that may include multinucleon interactions as

$$H = T_{\rm rel} + V. \tag{1}$$

By adopting a complete basis of Slater determinants, $|\Phi_j\rangle$ for A nucleons, developed from a chosen single-particle basis, we express the complete space problem as a matrix eigenvalue problem. That is, the eigenvalues E_k and eigenstates $|\Psi_k\rangle$, expanded in our complete basis of Slater determinants, obey

the equations

$$H|\Psi_k\rangle = E_k|\Psi_k\rangle, \quad (2)$$

$$|\Psi_k\rangle = \sum_j A_{kj}|\Phi_j\rangle, \quad (3)$$

where A_{kj} denotes the expansion coefficient.

The selection of the complete single-particle basis is flexible but we will follow a popular choice and adopt the three-dimensional HO due to its well-studied analytical properties that facilitate numerical applications and the retention of the underlying symmetries of H [7]. We take the neutron and proton mass m to be the same (938.92 MeV, their average measured mass), so that the only length scale in the HO single-particle basis can be expressed in terms of the HO energy $\hbar\Omega$ as

$$b = \sqrt{\frac{\hbar}{m\Omega}}. \quad (4)$$

B. Finite matrix truncation approach

In practical applications, it is advantageous to define the many-body truncation with $N_{\max}$, the maximum of the total HO quanta in the retained Slater determinants above the minimum total HO quanta for the A nucleons [7]. A quantum of the HO single-particle state is twice the radial quantum number n plus the orbital quantum number l. That minimum total HO quanta for the A nucleons also depends on the number of neutrons N and protons Z that comprise the system. Zero is the minimum total HO quanta for the two-nucleon systems addressed in this work.

We define the P space (or "model space") as the basis space retained by this $N_{\max}$ truncation. The infinite-dimensional space beyond this $N_{\max}$ truncation is called the Q space. For a sufficiently large $N_{\max}$, some observables are seen to converge in very light nuclei for interactions which do not couple strongly to high-momentum states and when computational resources are sufficient. For example, using a chiral N^{2}LO NN interaction [10,11], the ground-state energy of ^{6}Li has been calculated [12–14] in a sequence of HO basis spaces. With extrapolation to the complete basis, the result is $-31.0(2)$ MeV [14]. Here, the parenthesis specifies the uncertainty as 200 keV in the extrapolation. The basis-space truncation for the largest finite basis employed in the extrapolation is $N_{\max} = 18$. At $N_{\max} = 18$ and $\hbar\Omega = 28$ MeV the ground-state energy, which is also a variational upper bound of the exact result, is already -29.928 MeV, i.e., about 1.1 MeV above the extrapolated result. For comparison, the experimental ground-state energy is -31.995 MeV [15].

However, other observables, such as the root-mean-square (rms) point-proton radius and electric quadrupole transitions, converge poorly up through $N_{\max} = 18$ [16]. For long-range observables such as the rms point-proton radius, the theoretical results are insufficiently converged to provide directly a meaningful comparison with experiment. For example, with extrapolations, the rms point-proton radius for ^{6}Li has significant uncertainties [16].

For all these reasons, it may be advantageous to soften the interactions and to promote improved convergence of the eigenvalue problem. As we explain in the next section, this softening, or renormalization of the interaction also necessitates renormalizing the operators corresponding to these other observables. That is, we need to consistently derive the effective operators for all observables in the chosen model space.

C. Effective Hamiltonian and operators

Once the complete basis space and the P space are defined, we can address the development of an effective Hamiltonian H_{eff} for the P space that formally retains a subset of the eigenvalues of the complete space. We adopt the OLS method [1–3], which we briefly outline here. More details, including specifics for including three-nucleon interactions, are found in Ref. [7].

The formal structure of the OLS approach is visualized by first considering H in the complete basis space and defining the unitary transformation U that diagonalizes H to produce the Hamiltonian's spectral form H_d along with the P-space projection of U, which we denote as W^P,

$$H_d := UHU^\dagger, \quad (5)$$

$$W^P := PUP. \quad (6)$$

Provided that the projected eigenvectors form a complete set of linearly independent vectors in the P space, we can then construct a finite basis transformation $\widetilde{U}^P$, which is unitary in the P space, as

$$\widetilde{U}^P := \frac{W^P}{\sqrt{W^{P\dagger}W^P}}. \quad (7)$$

With this transformation, we define our H_{eff} for the P space with

$$H_{\text{eff}} := \widetilde{U}^{P\dagger}H_d\widetilde{U}^P, \quad (8)$$

$$= \widetilde{U}^{P\dagger}UHU^\dagger\widetilde{U}^P. \quad (9)$$

We denote the OLS transformation U_{OLS} by the combination

$$U_{\text{OLS}} := \widetilde{U}^{P\dagger}U. \quad (10)$$

We define our P space to accommodate the lowest set of eigenvalues of the original Hamiltonian though other choices are feasible, such as retaining states whose eigenvectors have the largest probabilities of P-space configurations. We furthermore note that H_{eff} is not unique since there is the freedom of a residual P-space unitary transformation that preserves H_d. Additional mathematical issues have been addressed in Ref. [17] such as the breakdown when linearly dependent projected eigenvectors are encountered. We did not encounter this breakdown in the calculations reported in this work. A central issue for the current work is to investigate the effects of the corresponding transformation on the observables O needed to generate consistent renormalizations. That is, we define consistent effective operators

$$O_{\text{eff}} := U_{\text{OLS}}OU_{\text{OLS}}^\dagger \quad (11)$$

for calculations of observables with the P-space eigenfunctions of $H_{\rm eff}$.[1]

While these steps provide the formal framework, the essential question of a practical implementation requires further discussion. In the NCSM, one introduces an auxiliary confining potential, which is later removed, and solves for the OLS transformations on a subset of the nucleons in the nucleus (typically two or three nucleons) in what is dubbed a "cluster approximation" [7,18]. The derived few-nucleon effective interaction is designed to renormalize the strong few-nucleon correlations in the presence of other nucleons approximated by the auxiliary potential. This effective interaction is subsequently employed to define an A-nucleon effective Hamiltonian. The cluster approximation is guaranteed to produce the exact results as either the cluster size is increased to reach the full A-nucleon system or as the P-space truncation is removed. The two-nucleon cluster approximation of the NCSM serves as a paradigm for introducing and solving the NN systems of this work. Our aim is to investigate the ramifications of this approach for effective electroweak operators derived in a manner consistent with the softened interaction.

To this stage, we have described the formal structure of the OLS method and we have discussed its applications within the NCSM. For the two-nucleon systems we address below, either without or with a HO trap, we apply the OLS approach in the relative coordinate system. Since the NN Hamiltonian is defined with the conserved symmetries of each NN partial wave (channel), we apply the OLS method to each NN channel independently. That is, we solve for individual OLS transformations in a relative HO basis of fixed total angular momentum, coupled spin, parity, and charge—the conserved quantum numbers for each NN channel. Then, we calculate the effective nonscalar operators with OLS transformations from the NN channels required for that operator. In these applications, the length scale of Eq. (4) is defined with the reduced mass, which we take to be 469.46 MeV for all NN channels.

III. APPLICATIONS TO TWO-NUCLEON SYSTEMS

A. Deuteron ground state

We define an initial system to consist of two nucleons described by the H of Eq. (1) whose ground-state energy we investigate in this subsection. Motivated by the NCSM cluster approximation framework, we will define a second two-nucleon system in the next subsection that adds a confining HO interaction (trap). Both systems are numerically solvable. We refer to the numerical solutions of these two systems as their "exact" results and we present these results in the Appendix. Using graphical representations, we compare these exact results with solutions from a truncation approach and with solutions from an OLS effective Hamiltonian approach. We refer to the results from the truncation approach and the results from the OLS approach each as "model" results.

We adopt NN interactions from chiral effective field theory (EFT) and we include the Coulomb interaction between proton pairs in the Hamiltonian. Specifically, we employ the NN interactions of the Low Energy Nuclear Physics International Collaboration (LENPIC) [10–14], which have been developed for each chiral order up through N^{4}LO. These LENPIC interactions employ a semilocal coordinate-space regulator and we select the interactions with the regulator range $R = 1.0$ fm [13,14]. We refer to these interactions as "LENPIC–X," where "X" defines the specific chiral order (LO, NLO, N^{2}LO, N^{3}LO, or N^{4}LO). We also employ the chiral EFT interaction of Ref. [19] with momentum-space regulator 500 MeV, which we refer to as "Idaho–N^{3}LO." All of these chiral EFT interactions are charge dependent.

We consider the neutron-proton (np) system since the deuteron ground-state provides the only bound NN state. In particular, we solve for the deuteron ground-state energy for each interaction using three approaches. First, we obtain a high-precision result by diagonalizing the Hamiltonian in the coupled $^3S_1$-$^3D_1$ channel in a very large HO basis ($N_{\rm max} = 400$) for three different values of the HO energy $\hbar\Omega$. We have verified that these ground-state energies produce the same result as the numerical solution of the Schroedinger equation to at least five significant figures [10,11] in all cases. We refer to these results from diagonalization at $N_{\rm max} = 400$ as the "exact" results. One may view these exact results as creating a discretized approximation to the continuum and we note that the largest eigenvalues exceed 1 GeV in all cases investigated here. Second, we solve for the ground-state energy in the HO bases truncated at lower $N_{\rm max}$ values to produce model results for the simple truncation approach. Third, we solve for the OLS effective Hamiltonian at each value of $N_{\rm max}$ and $\hbar\Omega$, following the methods described above, to produce the model results for the OLS approach. We follow this same approach for the neutron-neutron (nn) and proton-proton (pp) channels needed for some of the transitions addressed in this work.

The model results of the truncation and OLS approaches are used to calculate their fractional difference with respect to our exact results for each observable (i.e., observables calculated with the $N_{\rm max} = 400$ wave functions) where the fractional difference, Fract. Diff., is defined as the scaled difference (model − exact)/|exact|. The Fract. Diff. results for the deuteron ground-state energy are presented as curves in Fig. 1 for a representative selection of our NN interactions. We do not show the results for LENPIC-LO since they are similar to the LENPIC–NLO results. Also, we do not show the LENPIC–N^{4}LO results, which are similar to those of LENPIC–N^{3}LO.

From the results in Fig. 1, we observe that the convergence rates for the truncation approach can depend significantly on the chiral order with the LENPIC NN interaction. In particular, there is a dramatic slowing of the convergence rates at N^{3}LO as seen in Fig. 1(c) compared to Figs. 1(a) and 1(b). The dependence of the convergence rates on the LENPIC chiral orders is also revealed in many-body observables where

[1]Note that we are addressing a P space which generally includes eigenstates with different conserved quantum numbers. The $U_{\rm OLS}$ transformation will properly manage scalar operators that conserve the symmetries of H as well as nonscalar operators that may induce transitions between eigenstates.

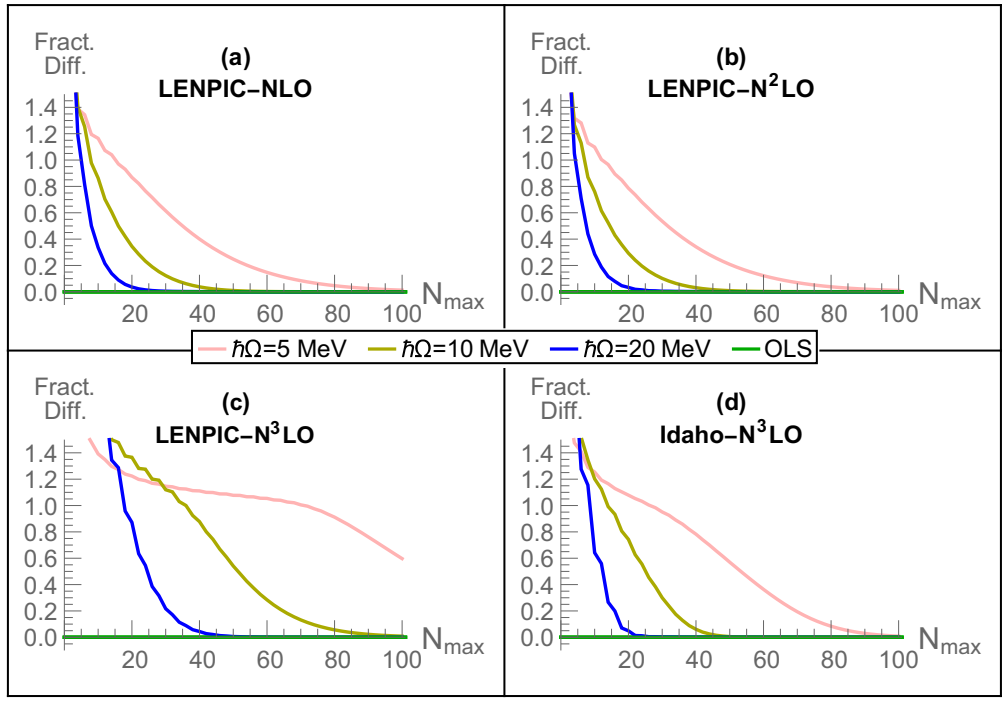

FIG. 1. The fractional differences, where Fract. Diff. of an observable = (model − exact)/|exact|, for the deuteron ground-state energy at three values of the HO energy $\hbar\Omega$ as a function of the P-space limit $N_{\max}$. The model results from diagonalizing the P-space truncated Hamiltonian matrix produce Fract. Diff. curves that decrease towards zero with increasing $N_{\max}$ in accordance with the variational principle. The model results from diagonalizing the OLS–renormalized Hamiltonian matrix reproduce the exact results at each $N_{\max}$ to high precision, yielding flat and overlapping green lines for their Fract. Diff. plots in all cases. Panels (a), (b) and (c) correspond to the Hamiltonians constructed with the LENPIC chiral EFT interactions [10–14] at NLO, N^{2}LO, and N^{3}LO, respectively. We employ the LENPIC interactions with coordinate-space regulator $R = 1.0$ fm. Panel (d) corresponds to the Hamiltonian constructed with the Idaho–N^{3}LO potential [19] with momentum-space regulator 500 MeV. The exact ground-state energies are given in Table I of the Appendix.

slower convergence leads to larger extrapolation uncertainties [12–14].

Comparing the LENPIC NN interaction results in Fig. 1 also reveals changing shapes of the convergence patterns with increasing chiral order for the bases using HO energy $\hbar\Omega =$ 5 and 10 MeV. In particular, the case with $\hbar\Omega = 5$ MeV develops a region showing significantly reduced slope, nearly a plateau, with increasing $N_{\max}$ at N^{3}LO [Fig. 1(c)]. The results for the Idaho–N^{3}LO interaction shown in Fig. 1(d) indicate convergence patterns intermediate to LENPIC–N^{2}LO [Fig. 1(b)] and LENPIC–N^{3}LO [Fig. 1(c)]. These regions of reduced slope correspond to Fract. Diff ≈ 1.0, which defines a region of P spaces where the lowest solution is transitioning between an unbound state and a bound state with increasing $N_{\max}$. Thus, for some interactions at lower values of $\hbar\Omega$, we observe a plateaulike behavior as seen in Figs. 1(c) and 1(d). In these same cases, after crossing over to a bound-state solution, the convergence rate accelerates. We have investigated this plateau and have found a correlation with a changing feature of the wave function: While the solution is moving across the plateau with increasing $N_{\max}$ it is building up its d-state component from near zero to near its final value. When it nearly acquires its final value, the energy decreases to a bound state (Fract. Diff. falls below 1.0) and accelerates its convergence rate. We examined other interactions exhibiting this plateau in Fract. Diff. and found a similar correlation with buildup of the d-state probability. We anticipate that, at sufficiently low values of the basis $\hbar\Omega$, we would find a similar plateau with all realistic interactions for the deuteron.

The dependence of the convergence rate on the basis $\hbar\Omega$ for the truncation approach in Fig. 1 is systematic—from most rapid convergence at $\hbar\Omega = 20$ MeV to slowest at $\hbar\Omega = 5$ MeV. We have not sought to optimize the choice of $\hbar\Omega$, although that is often a point of interest in many-body applications. Our interest here is rather to feature results for a range of choices of $\hbar\Omega$ that will be useful for our investigation of electroweak observables in the system of the following subsection.

The Fract. Diff. for the results of the OLS approach in Fig. 1 always remains at zero, to within our numerical precision, which is what one anticipates. That is, since the OLS approach should provide the exact ground-state energy in any basis space, these results serve as a verification of our numerical procedures. The OLS procedure reproduces that subset of eigenvalues of the complete problem compatible with the dimensionality fixed by $N_{\max}$, including eigenvalues lying high in the continuum. We verify the accuracy of the eigenvalues from the OLS approach by direct comparison with the corresponding subset of results from the complete problem for each set of P-space basis parameters. We have confirmed that our OLS eigenvalues agree with the respective subset of the exact eigenvalues to at least six significant figures.

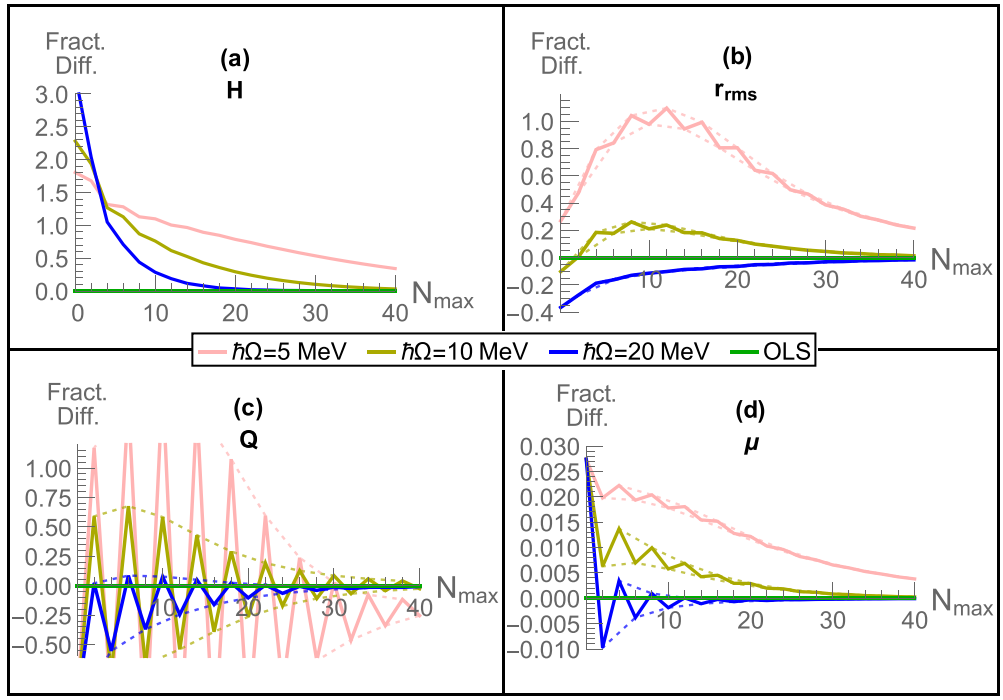

FIG. 2. The fractional differences for a selection of deuteron properties at three values of the HO energy basis parameter $\hbar\Omega$ as a function of the P-space limit $N_{\max}$. Following the scheme of Fig. 1, we present the Fract. Diff. for the truncated basis calculations (three colored curves approaching zero at high $N_{\max}$) and for the OLS renormalized calculations (green curves all coincident with zero). All results are obtained with the LENPIC–N^{2}LO interaction with regulator $R = 1.0$ fm. The ground-state energy in panel (a) is an expanded version of the ground-state energy in panel (b) of Fig. 1. The rms point-proton radius $r_{\rm rms}$ appears in panel (b), the electric quadrupole moment Q in panel (c) and the magnetic moment μ in panel (d). The model results using the OLS transformation method reproduce the exact results at each $N_{\max}$ to high precision, yielding flat and overlapping green lines for their Fract. Diff. plots in all cases. The short dashed lines provide envelopes for results with sawtooth patterns. The exact values used for the observables here are given in Table II of the Appendix.

We now present additional observables for the deuteron that represent baseline results for later comparison. In Fig. 2 we show the ground-state energy [Fig. 2(a)], rms point-proton radius [Fig. 2(b)], electric quadrupole moment [Fig. 2(c)], and magnetic moment [Fig. 2(d)] for the same set of 3 HO basis parameters as in Fig. 1 using the LENPIC–N^{2}LO interaction. Here, we expand the scale to see details of the results from $N_{\max} = 0$–40. Clearly, the results in the truncated basis exhibit strong deviations from their exact values and those deviations exhibit nonsmooth behavior, such as sawtooth patterns, with increasing $N_{\max}$. The excursions in the electric quadrupole moment in Fig. 2(c) are especially prominent. These features represent the role of an s-state plus d-state combination that are added with each increase in $N_{\max}$ by 2 units. With the addition of two such combinations (increase $N_{\max}$ by four units) we include states with canceling asymptotic tails. This observation helps one to understand why results differing by 4 units in $N_{\max}$ follow a simpler trend in Fig. 2—a trend visualized by the dotted line connecting the successive maxima and another dotted line connecting the successive minima of the sawtooth patterns. Such a visualization is also applied to the maxima and the minima of the sawtooth patterns of the other observables in Fig. 2, the rms radius (b) and magnetic moment (c). Note that the scale for the magnetic moment is greatly enlarged relative to the other scales in Fig. 2 indicating it is rather insensitive to basis truncation effects.

Here again, the calculations of the effective operators with the OLS method, when employed with the OLS wave functions in the same P space, provide the exact results to within six digits for each observable at each value of the trap. The OLS results are seen as the flat green lines at Fract. Diff. ≈ 0 in Fig. 2.

B. Two nucleons in HO trap—Ground-state energy

For the purpose of investigating effective electroweak operators and gauging a range of representative behaviors anticipating future applications to finite nuclei, we augment the initial system of the previous subsection with the addition of a confining interaction or trap. We adopt a HO confining potential and separate the effects of the trap into center-of-mass and relative motion. Since the center-of-mass motion factorizes, its wave function is an exact HO eigenstate and not affected by the NN interaction acting in relative coordinates. We subsequently consider only the relative motion of the two nucleons in the confining HO potential of relative motion and employ the Hamiltonian:

$$H = T_{\rm rel} + V + \tfrac{1}{2}\mu\Omega^2 r^2. \tag{12}$$

For these systems, we adopt HO energies for the confining interaction which match the basis values of $\hbar\Omega = 5$, 10, and 20 MeV introduced above.

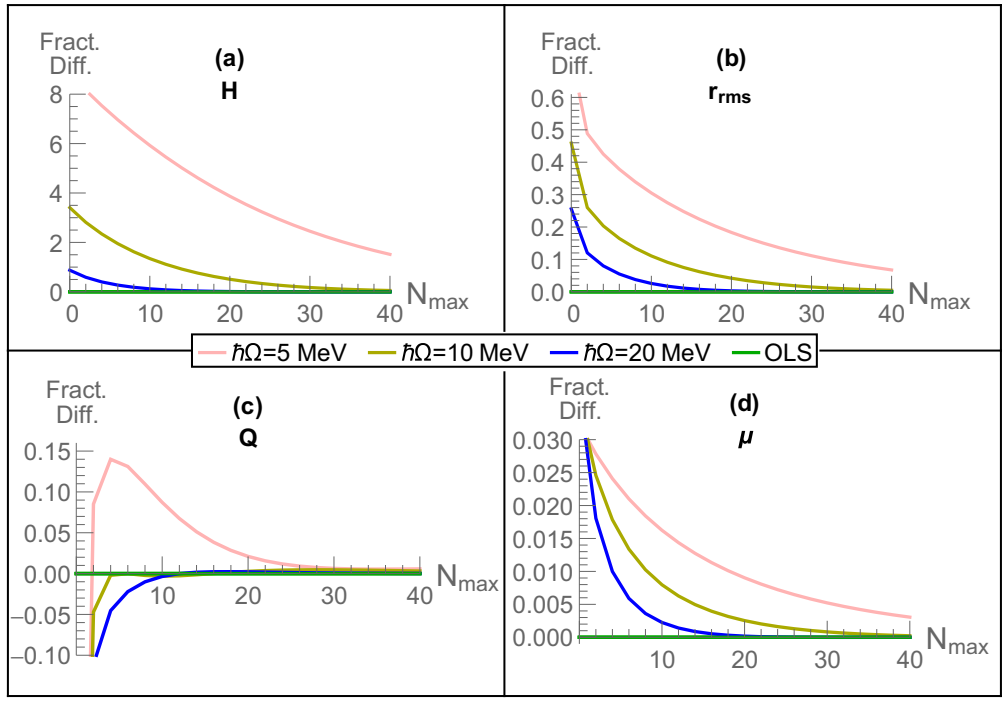

FIG. 3. Fractional differences between model and exact results as a function of the P space for selected ground-state observables of the two-nucleon system in the ${}^3S_1$-${}^3D_1$ channel for three different HO traps. The NN interaction is the LENPIC–N^{2}LO NN interaction with regulator $R = 1.0$ fm. HO energies $\hbar\Omega$ for the bases correspond to the HO energies of the traps. The observables correspond to the eigenenergy (a), the rms point-proton radius (b), the electric quadrupole moment (c), and the magnetic dipole moment (d). The exact values used for the observables here are given in Table III of the Appendix.

In this second system, the HO trap simulates the role of the nuclear medium in which the two-nucleon subsystem is embedded. For applications where we expect weakly bound nucleons to dominate the electroweak properties, we provide results with the confining strength parameter $\hbar\Omega = 5$ MeV. Then we progress to simulate contributions from moderately bound to deeply bound nucleon pairs with $\hbar\Omega = 10$ and 20 MeV, respectively. We also note that the addition of the HO trap emulates the mathematical framework for the two-body cluster approximation in the NCSM where the HO trap is added during the development of the effective Hamiltonian and then removed at the stage of defining the effective interaction [7]. Such a treatment of the HO trap as a pseudopotential is known to improve convergence in NCSM applications with the OLS approach using the cluster approximation. We therefore anticipate that studying the two-nucleon system with various HO traps, including its electroweak properties, will provide insights into renormalization effects on observables in future NCSM applications to finite nuclei.

For simplicity, we elect to retain only a subset of the LENPIC NN interactions for this second system. In Fig. 3(a) we show the Fract. Diff. for the ground-state energy in the ${}^3S_1$-${}^3D_1$ channel for the three different traps. Again, we list the exact results in the Appendix. Note that, for this second system, the exact results depend on the HO strength parameter $\hbar\Omega$. The convergence rate for results of the truncation approach is again systematic—slowest with $\hbar\Omega = 5$ MeV and fastest with $\hbar\Omega = 20$ MeV. However, the scale for Fract. Diff. in Fig. 3(a) is much larger than in Fig. 1. Nevertheless, the results of the OLS approach again provide agreement with the exact ground-state energy results over all choices of P space as evident by the coincident flat green lines at Fract. Diff. $= 0$.

C. Two nucleons in HO trap—Electromagnetic observables

We now turn our attention to additional observables in this second system where we again aim to compare the results of the truncation approach with those of the OLS approach. We note that a consistent OLS treatment of various long-range observables has been investigated in the past and results of truncation versus OLS approaches have been shown to be in the range from a few percentages to about 10% [4–6]. Our aim here is to investigate both electromagnetic and weak observables over a wide range of basis spaces but in the limited two-nucleon system. In the end, we find large effects for matrix elements of some observables in cases with traps having small HO energies and/or in cases having small $N_{\max}$ values. This suggests that truncation effects are more severe and renormalization effects are more important when approaching observables involving weakly bound states and transitions involving resonance states.

For the initial set of ground-state observables beyond the ground-state energy, we again examine the rms point-proton radius $r_{\rm rms}$, quadrupole moment Q, and magnetic dipole moment μ. We note that the role of the harmonic confining interaction is significant since the wave functions will therefore have gaussian asymptotic properties which moderate the long-range contributions of these operators. In true nuclear bound state environments, the asymptotic wave functions are

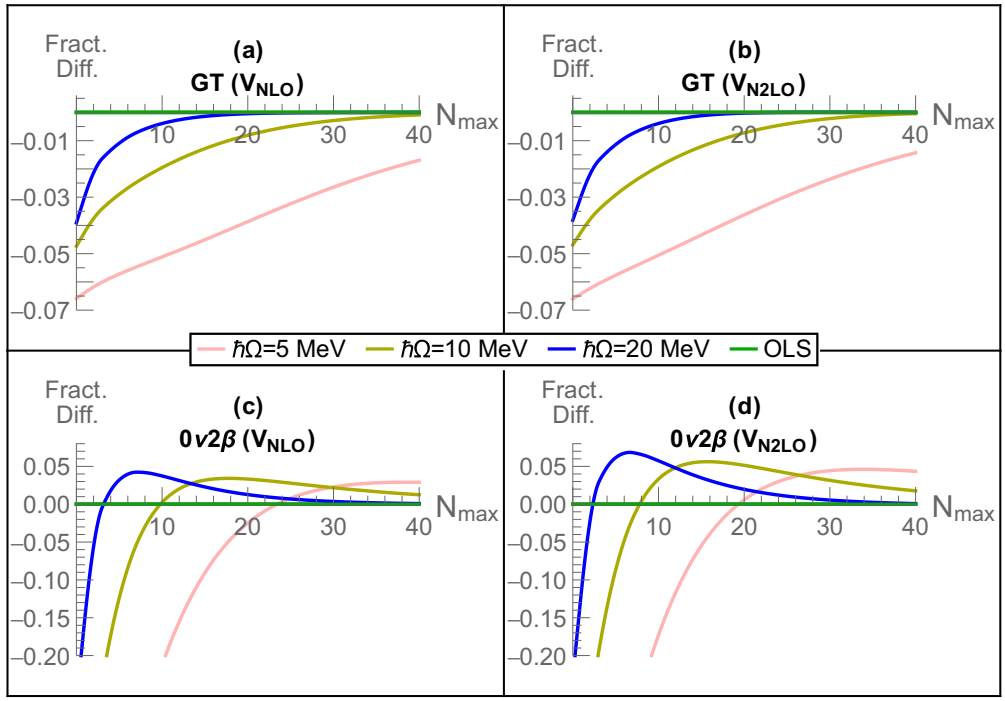

FIG. 4. Fractional differences between model and exact results as a function of the P space for selected ground-state transitions from the lowest state of the $^1S_0$ nn system in three different HO traps. Panels (a) and (b) are for the allowed GT transition to the ground state of the $^3S_1$-$^3D_1$ channel. Panels (c) and (d) are for the $0\nu2\beta$ decay to the ground state of the $^1S_0$ pp system. The NN interaction for cases (a) and (c) are taken to be the LENPIC–NLO potential, while we adopt the LENPIC–N^{2}LO potential for cases (b) and (d). All results shown employ LENPIC NN interactions with coordinate space regulator $R = 1.0$ fm. The exact values used for the observables here are given in Table IV of the Appendix.

exponential and provide significant contributions to the long-range observables.

For both the truncation approach and the OLS approach, we again present the results for the ground-state expectation value of these operators as a fractional difference from the exact results in Fig. 3. The exact results are, again, those obtained in $N_{\max} = 400$ calculations and are given in the Appendix for completeness. Note the major differences in the scales of Fig. 3. The results of truncation are the largest for the ground-state energy (see discussion above) and then decreasing in size for $r_{\rm rms}$, Q, and μ in that order. The results of truncation are also largest at $\hbar\Omega = 5$ MeV and smallest at $\hbar\Omega = 20$ MeV. Physically, one expects that, as $\hbar\Omega$ increases, the trap will become more important than the NN interaction in the Hamiltonian. With this decreasing role of the NN interaction, results from the truncation approach will trend towards the simpler situation of two nucleons in a simple HO Hamiltonian where they are increasingly representative of the exact results with the same simple Hamiltonian. Indeed, the main impression of the results of the truncation approach with a trap in Fig. 3 is the generally smooth trends that contrast the results without a trap presented in Fig. 2—in particular, the sawtooth behavior seen in Fig. 2 is absent from Fig. 3. While $r_{\rm rms}$ [Fig. 3(b)] and μ [Fig. 3(d)] appear to have a monotonic convergence pattern, just like the ground-state energy, the convergence pattern for Q is slightly more complicated. The Fract. Diff. for Q in the truncation approach at lower HO trap energies exhibits a sign change while it exhibits a tendency towards monotonic behavior at larger trap energies.

As shown previously in Fig. 2, we find that, as expected, the results for the ground-state observables in Fig. 3 within the OLS approach agree with the exact ground-state results over all choices of P spaces and traps. This agreement is evident through the Fract. Diff. remaining zero (flat green lines) for the OLS results in all panels. We checked that the Fract. Diff. for the OLS results shown in Fig. 3 are zero to at least six significant figures.

D. Two nucleons in HO trap—Weak observables

We now consider the Gamow-Teller (GT) β-decay matrix element for the transition from the ground state of the $^1S_0$ nn channel to the ground state of the $^3S_1$-$^3D_1$ deuteron channel shown in Figs. 4(a) and 4(b) for the same traps as above. For Fig. 4(a) [and for Fig. 4(c)] we adopt the LENPIC–NLO NN interaction. For Fig. 4(b) [and for Fig. 4(d)] we adopt the LENPIC–N^{2}LO NN interaction. The GT operator is the simple spin-isospin form [20]. Our aim is to explore the role of two different, but lower, chiral order interactions with Figs. 4(a) and 4(b) [and also Fig. 4(c) and 4(d)]. Future works will employ GT operators from chiral EFT where the emphasis will shift to having all observables, including the eigenvalues, obtained with chiral EFT operators at the same chiral order.

The Fract. Diff. for the GT matrix elements in Figs. 4(a) and 4(b) displays convergence patterns in the truncation approach similar to the operators in Figs. 3(a), 3(b) and 3(d)

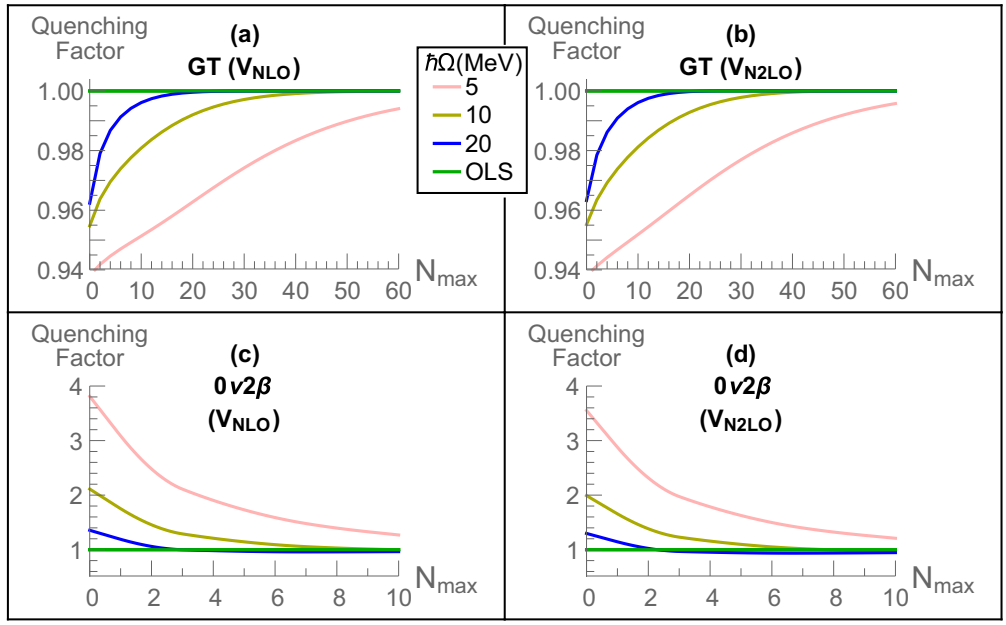

FIG. 5. Quenching factor defined as exact/model for GT-decay and $0\nu2\beta$-decay matrix elements as a function of the P space for ground-state transitions from the lowest state of the $^1S_0$ nn system in three different HO traps. Panels (a) and (b) are for the allowed GT-transition to the ground state of the $^3S_1$-$^3D_1$ channel. Panels (c) and (d) are for the $0\nu2\beta$ decay to the ground state of the $^1S_0$ pp system. The NN interaction for cases (a) and (c) are taken to be the LENPIC–NLO potential, while we adopt the LENPIC–N^{2}LO potential for cases (b) and (d). All results shown employ LENPIC NN interactions with coordinate space regulator $R = 1.0$ fm. A quenching factor greater than unity signals an enhancement of the model results is required to arrive at the exact results. The exact values used for the observables here are given in Table IV of the Appendix.

but on a reduced scale and with the opposite sign. The exact result, whose overall sign is arbitrary and has no physical consequence, is negative with our numerical procedures (see the Appendix). With increasing P-space dimension, the truncation results rise towards the exact results from below producing the Fract. Diff. trends for the GT matrix elements. Thus, in smaller basis spaces, the results of the truncation approach for this ground-state-to-ground-state transition would require the application of a scaling, or quenching factor, that is less than unity in order to match the exact results. In order to help make this point more clear, we present plots of the quenching factor (defined as the exact/model result) in Fig. 5 for the results in Fig. 4. We note in Figs. 5(a) and 5(b) that the quenching factor in truncated calculations of the GT matrix element deviates from unity by, at most, about 6%. The largest deviations from unity and the slowest convergence rates are found with the weakest HO trap energy of $\hbar\Omega = 5$ MeV where the nn and np ground states are spread in coordinate space compared with their distributions in the other HO traps. This systematic decrease of the GT quenching factor from unity with increasing spatial distribution of the two-nucleon system is reminiscent of the approximate phenomenological decrease in the quenching factor for GT matrix elements in valence spaces with increasing atomic number [21]. On the other hand, as expected, the OLS approach again produces the exact GT results for all our choices of the HO trap energies and for all choices of P-space [flat green lines at zero (unity) for Figs. 4(a) and 4(b) (Fig. 5)].

Finally, due to intense current interest, we investigate the $0\nu2\beta$-decay operator within the same approaches and exhibit the results for three traps in Figs. 4(c) and 5(c) (with LENPIC–NLO) and Figs. 4(d) and 5(d) (with LENPIC–N^{2}LO). We adopt the $0\nu2\beta$-decay operator from chiral EFT of Ref. [22], which is consistent with chiral N^{2}LO. For calculating our exact results, we employ a basis space with $N_{\max} = 200$ which is sufficient for high-precision calculations with the LENPIC interaction at N^{2}LO. We elect not to apply the LENPIC semilocal coordinate space regulator to this $0\nu2\beta$-decay operator as this regulator is not gauge invariant.

The $0\nu2\beta$-decay results in Fig. 4(c) and 5(c) and Figs. 4(d) and 5(d) reveal that convergence patterns of the truncation approach are sensitive to the HO energy of the trap. Furthermore, in contrast with several results seen above, the $0\nu2\beta$-decay Fract. Diff. results of Fig. 4 do not appear to approach the exact result with increasing P-space dimension until we reach about $N_{\max} = (10, 20, 40)$ for $\hbar\Omega = (20, 10, 5)$ MeV, respectively. At $N_{\max} = 0$, the magnitude of the results from the truncation approach are much smaller than the exact results; with increasing $N_{\max}$ the results from the truncation approach increase but overshoot the exact results by about 5% before converging towards the exact results. That is, at small $N_{\max}$ values, the $0\nu2\beta$-decay results with the truncation approach are significantly suppressed, indicating large effects due to evaluating matrix elements of this operator in truncated basis spaces. For more details of this lower region of $N_{\max}$, we turn to Figs. 5(c) and 5(d).

The quenching factors in the truncated calculations of $0\nu2\beta$ decay in Figs. 5(c) and 5(d) rise significantly above unity in the low $N_{\max}$ region contrary to what we find for the GT matrix elements. The rise is largest with the weakest trap

strength of $\hbar\Omega = 5$ MeV and smallest with the strongest trap of $\hbar\Omega = 20$ MeV. We interpret these results to indicate that significant contributions from intermediate range components of the $0\nu2\beta$-decay operator are omitted with truncations to the smaller model spaces. Furthermore, these results suggest that truncated calculations of $0\nu2\beta$ transition matrix elements between weakly bound nucleons are likely to require quenching factors greater than unity (i.e., enhancements) in small model spaces. In other words, these substantial excursions above unity may have significant implications for eventual applications in finite nuclei. It is also worth remarking that the OLS transformation is different for the initial and final states of both the GT and $0\nu2\beta$ matrix elements. Therefore, obtaining the exact results for these matrix elements for all P spaces by the OLS method is another nontrivial test of our numerical procedures.

IV. SUMMARY AND OUTLOOK

Our initial application to the deuteron ground state revealed the order-of-magnitude effects of simple P-space basis truncations compared with exact results as a function of the basis HO energy $\hbar\Omega$ for a set of realistic NN interactions. The smallest value studied, $\hbar\Omega = 5$ MeV, produced the largest truncation effects (hence the largest renormalization effects) for these interactions. We also showed that, for a wide range of P spaces and a selection of NN interactions, the Okubo-Lee-Suzuki approach consistently reproduced the exact results which one anticipates from a theoretical perspective.

Effective Hamiltonians and effective electroweak operators were then calculated for two nucleons in a confining harmonic oscillator trap as a function of the P space. For this system, matrix elements of all OLS-derived effective operators again agree with exact results in all model spaces and for all traps investigated. We quantify the deviations of the simple truncated space results from the exact results for three different traps as a function of the P space. We illustrate these effects for the root-mean-square point-proton radius, electric quadrupole moment, magnetic dipole moment, Gamow-Teller transition and neutrinoless double-β decay operators using NN interactions from chiral effective field theory.

From the results shown in Figs. 3–5, we found that the size of error in the matrix element of an observable introduced by a truncated basis space approach depends on the observable, the value of the HO parameter of the trap $\hbar\Omega$, and the severity of the P-space truncation given by $N_{\max}$. Long-range observables, such as the root-mean-square point-proton radius and the electric quadrupole moment exhibited larger errors due to truncation to smaller spaces than the magnetic dipole and GT operators. We also found surprisingly large truncation errors for the neutrinoless double-β decay operator—larger than that of Q, and of the same order as the $r_{\rm rms}$ radius. On the other hand, the GT operator exhibited behaviors similar to the magnetic moment as may be expected.

While these results appear to be reasonable in the qualitative sense and are consistent with previous investigations, the quantitative dependences shown here may be useful in estimating uncertainties for observables obtained in truncated many-body calculations with realistic NN interactions. In particular, since renormalization effects tend to be larger in cases with weaker traps and smaller basis spaces, applications to heavier nuclei, for both transitions between weakly bound nucleons and to continuum states, will likely be subject to the more significant renormalization effects.

The results presented here also signal the approximate magnitude of the corrections that the OLS renormalization provides for each of our selected observables. These corrections, which can be obtained with OLS renormalization, should be carried forward to the appropriate many-body applications. It will also be important to implement the chiral effective field theory treatment of the electroweak operators that are consistent with the chiral effective field theory of the strong internucleon interactions.

ACKNOWLEDGMENTS

We acknowledge fruitful discussions with Hugh Potter, Evgeny Epelbaum, Hermann Krebs, and Jacek Golak. We thank Angelo Calci for harmonic oscillator matrix elements of the LENPIC interactions. This work was supported in part by the U.S. Department of Energy (DOE) under Grants No. DE-FG02-87ER40371, No. DE-SC0018223 (SciDAC-4/NUCLEI), and No. DE-SC0015376 (DOE Topical Collaboration in Nuclear Theory for Double-Beta Decay and Fundamental Symmetries). P.M. thanks the Fundação de Amparo à Pesquisa do Estado de São Paulo (FAPESP) for support under Grant No. 2017/19371-0. Computational resources were provided by the National Energy Research Scientific Computing Center (NERSC), which is supported by the U.S. Department of Energy (DOE) Office of Science under Contract No. DE-AC02-05CH11231.

APPENDIX

We present in Tables I through IV the "exact" results that correspond to the $N_{\max} = 400$ case unless otherwise specified, where all results have converged to six or more digits of precision as a function of $N_{\max}$. All results involving the LENPIC interactions in the Hamiltonian correspond to adopting the LENPIC regulator $R = 1.0$ fm. Results are presented at each value of the HO basis parameter $\hbar\Omega$ and for each observable. Differences between the "exact" results in the sixth significant figure at different values of $\hbar\Omega$ in Tables I and II arise from the transformation of the HO basis representation from an initial representation at $\hbar\Omega = 28$ MeV where 5 significant figures in the ground-state energy was adopted as the criteria for accuracy in the HO basis transformation. On the other hand, the results shown here to six significant figures are the results reproduced by the OLS transformation to at least this level of accuracy. The differences between the three columns in Tables III and IV are due to the different confining potentials. Note that the sign for the transition matrix elements in Table IV is arbitrary.

TABLE I. Ground-state eigenvalues (in MeV) for the specified potentials used as the "exact" values in Fig. 1 as a function of the basis parameter $\hbar\Omega$.

	$\hbar\Omega$ (MeV)		
Potential	5	10	20
LENPIC–NLO	−2.20607	−2.20609	−2.20609
LENPIC–N^{2}LO	−2.23508	−2.23516	−2.23516
LENPIC–N^{3}LO	−2.22324	−2.22326	−2.22326
Idaho–N^{3}LO	−2.22458	−2.22459	−2.22458

TABLE II. Ground-state eigenvalues and selected observables used as the "exact" values in Fig. 2 as a function of the basis parameter $\hbar\Omega$. The results were obtained with the LENPIC–N^{2}LO interaction with regulator $R = 1.0$ fm. No confining interaction was included.

	$\hbar\Omega$ (MeV)		
Ground-state observable	5	10	20
H (MeV)	− 2.23508	− 2.23516	− 2.23516
$r_{\rm rms}$ (fm)	1.96440	1.96436	1.96436
Q (e fm^2)	0.269862	0.269874	0.269873
μ (μ_N)	0.856323	0.856323	0.856323

TABLE III. Ground-state eigenvalues and selected observables used as the "exact" values in Fig. 3. The results were obtained with the LENPIC–N^{2}LO interaction with regulator $R = 1.0$ fm. The strength of the confining HO potential is the same as the basis parameter $\hbar\Omega$ that labels each column of results.

	$\hbar\Omega$ (MeV)		
Ground-state observable	5	10	20
H (MeV)	− 0.703487	2.35148	10.7332
$r_{\rm rms}$ (fm)	1.44078	1.20869	0.992923
Q (e fm^2)	0.204165	0.164676	0.122359
μ (μ_N)	0.852184	0.849597	0.84814

TABLE IV. Ground-state transition matrix elements used as the "exact" values in Figs. 4 and 5. The strength of the confining HO potential is the same as the basis parameter $\hbar\Omega$ that labels each column of results. The GT transition matrix element values correspond to the $N_{\rm max} = 400$ case, where they have converged to six or more significant digits. The $0\nu2\beta$ transition matrix element values correspond to the $N_{\rm max} = 200$ case, where they have converged to four or more significant digits.

		$\hbar\Omega$ (MeV)		
Decay	LENPIC	5	10	20
GT	NLO	− 1.40355	− 1.42839	− 1.43974
	N^{2}LO	− 1.40338	− 1.42902	− 1.44106
$0\nu2\beta$	NLO	1.59067	0.505287	0.827882
	N^{2}LO	1.48274	0.476412	0.792684

[1] S. Okubo, Prog. Theor. Phys. **12**, 603 (1954).
[2] K. Suzuki and S. Y. Lee, Prog. Theor. Phys. **64**, 2091 (1980).
[3] K. Suzuki, Prog. Theor. Phys. **68**, 246 (1982).
[4] I. Stetcu, B. R. Barrett, P. Navrátil, and J. P. Vary, Phys. Rev. C **71**, 044325 (2005).
[5] I. Stetcu, B. R. Barrett, P. Navrátil, and J. P. Vary, Phys. Rev. C **73**, 037307 (2006).
[6] A. F. Lisetskiy, M. K. G. Kruse, B. R. Barrett, P. Navrátil, I. Stetcu, and J. P. Vary, Phys. Rev. C **80**, 024315 (2009).
[7] B. R. Barrett, P. Navrátil, and J. P. Vary, Prog. Part. Nucl. Phys. **69**, 131 (2013).
[8] E. Dikmen, A. F. Lisetskiy, B. R. Barrett, P. Maris, A. M. Shirokov, and J. P. Vary, Phys. Rev. C **91**, 064301 (2015).
[9] E. R. Anderson, S. K. Bogner, R. J. Furnstahl, and R. J. Perry, Phys. Rev. C **82**, 054001 (2010).
[10] E. Epelbaum, H. Krebs, and U.-G. Meißner, Phys. Rev. Lett. **115**, 122301 (2015).
[11] E. Epelbaum, H. Krebs and U.-G. Meißner, Eur. Phys. J. A **51**, 53 (2015).
[12] P. Maris, S. Binder, A. Calci, E. Epelbaum, R. J. Furnstahl, J. Golak, K. Hebeler, H. Kamada, H. Krebs, J. Langhammer, S. Liebig, U.-G. Meißner, D. Minossi, A. Nogga, H. Potter, R. Roth, R. Skibiński, K. Topolnicki, J. P. Vary, and H. Witala, EPJ Web Conf. **113**, 04015 (2016).
[13] S. Binder, A. Calci, E. Epelbaum, R. J. Furnstahl, J. Golak, K. Hebeler, H. Kamada, H. Krebs, J. Langhammer, S. Liebig, P. Maris, U.-G. Meißner, D. Minossi, A. Nogga, H. Potter, R. Roth, R. Skibinski, K. Topolnicki, J. P. Vary, and H. Witala (LENPIC Collaboration), Phys. Rev. C **93**, 044002 (2016).
[14] S. Binder, A. Calci, E. Epelbaum, R.J. Furnstahl, J. Golak, K. Hebeler, T. Hüther, H. Kamada, H. Krebs, P. Maris, U.-G. Meißner, A. Nogga, R. Roth, R. Skibinski, K. Topolnicki, J. P. Vary, K. Vobig, and H. Witala (LENPIC Collaboration), Phys. Rev. C **98**, 014002 (2018).
[15] D. R. Tilley, C. M. Cheves, J. L. Godwin, G. M. Hale, H. M. Hofmann, J. H. Kelley, C. G. Sheu, and H. R. Weller Nucl. Phys. A **708**, 3 (2002).
[16] I. J. Shin, Y. Kim, P. Maris, J. P. Vary, C. Forssen, J. Rotureau, and N. Michel, J. Phys. G **44**, 075103 (2017).
[17] C. P. Viazminsky and J. P. Vary, J. Math. Phys. **42**, 2055 (2001).
[18] P. Navrátil, J. P. Vary, and B. R. Barrett, Phys. Rev. Lett. **84**, 5728 (2000).
[19] D. R. Entem and R. Machleidt, Phys. Rev. C **68**, 041001 (2003).
[20] A. Bohr and B. Mottelson, *Nuclear Structure* (World Scientific, Singapore, 1998), Vol. 1, p. 407.
[21] G. Martinez-Pinedo, A. Poves, E. Caurier, and A. P. Zuker, Phys. Rev. C **53**, R2602 (1996).
[22] G. Prezeau, M. Ramsey-Musolf, and P. Vogel, Phys. Rev. D **68**, 034016 (2003).